

# **A Rheology Model of High Damping Rubber Bearings for Seismic Analysis: Identification of nonlinear viscosity**

*A.R. Bhuiyan<sup>a\*</sup>, Y. Okui<sup>a</sup>, H. Mitamura<sup>b</sup>, T. Imai<sup>c</sup>*

*<sup>a</sup> Department of Civil and Environmental Engineering  
Saitama University, Saitama 338-8570, Japan*

*<sup>b</sup> Civil Engineering Research Institute for Cold Region, PWRI, Sapporo 062-8602,  
Japan*

*<sup>c</sup> Rubber Bearing Association, Tokyo 107-0051, Japan*

---

## **\*Corresponding Author:**

Abdur Rahman Bhuiyan

Department of Environmental Science and Civil Engineering, Saitama University  
255 Shimo Okubo, Saitama 338-8570, Japan

E-mail address: [s06de056@mail.saitama-u.ac.jp](mailto:s06de056@mail.saitama-u.ac.jp); [arbhuiyan@yahoo.com](mailto:arbhuiyan@yahoo.com)

Tel.: +81 48 858 3558; Fax: +81 48 858 3558

## **Abstract**

The mechanical behavior of high damping rubber bearings (HDRBs) is investigated under horizontal cyclic shear deformation with a constant vertical compressive load. On the basis of experimental observations, an elasto-viscoplastic rheology model of HDRBs for seismic analysis is developed. In this model, the Maxwell model is extended by adding a nonlinear elastic spring and an elasto-plastic model (spring-slider) in parallel. In order to identify constitutive relations of each element in the rheology model, an experimental scheme comprised of three types of tests, namely a cyclic shear (CS) test, a multi-step relaxation (MSR) test, and a simple relaxation (SR) test, are carried out at room temperature. HDRB specimens with the standard ISO geometry and three different high damping rubber materials are employed in these tests. A nonlinear viscosity law of the dashpot in the Maxwell model is deduced from the experimental scheme, and incorporated into the rheology model to reproduce the nonlinear rate dependent behavior of HDRBs. Finally, numerical simulation results for sinusoidal loading are presented to illustrate capability of the proposed rheology model in reproducing the mechanical behavior of HDRBs.

Key words: High damping rubber bearing; Rheology model; Nonlinear viscosity; Over stress; Loading and unloading; Seismic response.

## **1. Introduction**

Destructive earthquakes and wind-induced vibrations always remind us to the need for better and more effective ways of mitigating these hazards. Recent earthquakes occurred in Northridge, USA in 1994 and Kobe, Japan in 1995 etc., which have shown the inadequacy of the design of existing structures, led engineers rethink widely on how to design structures against earthquakes. At present, in the seismic design and retrofit of structures, a seismic isolation approach is widely adopted owing to its economical efficiency. In this approach, the ductility demand of structural elements can be reduced thereby installing isolation devices between the superstructure and the substructure. The isolation devices are basically classified into sliding bearings and laminated rubber bearings. The sliding bearings are introduced to filter out the imparting earthquake forces by providing frictional sliding. On the other hand, the laminated rubber bearings with high flexibility are meant to shift the natural period of structures so as to avoid the resonance with excitations; they are usually endowed/accompanied with some damping properties to prevent the isolated structures from over-displacing.

The laminated rubber bearings have seen more and more applications in recent years as seismic isolation devices in bridges. Three types of laminated rubber bearings are widely used for this purpose: natural rubber bearing (NRB), lead rubber bearing (LRB), and high damping rubber bearing (HDRB). Of these bearings, the use of HDRB as the seismic isolation device in bridges is increased due to its enhanced dissipation property. HDRB is composed of alternating layers of rubbers and steel shims, and the rubber layers are

reinforced by the steel shims. The reinforcing steel shims constrain the rubber layers from lateral expansion and provide high vertical stiffness, but have no effect on the shear stiffness (Salomon et. al., 1999; Skinner, 1993).

Some guide specifications (AASHTO, 2000; JRA, 1996, 2002) for the seismic design of bridges with HDRBs have been developed. In these specifications, the nonlinear characteristics of HDRBs are expressed in terms of a bilinear model. However, the past investigation conducted by some authors (Dall's Asta and Ragni, 2006; Hwang et al., 2002) have indicated that the mechanical behavior of HDRBs is characterized by strain-rate-dependent hysteresis property. As an example, typical shear stress-strain responses of a HDRB are presented in Fig.1, where the strain-rate dependency of hysteresis is clearly illustrated. Relatively strong strain-rate dependency is observed in loading than in unloading. Furthermore, the strain hardening behavior is also illustrated in Fig.1 (see, also Abe et al., 2004a). The current bilinear model used in design practice cannot represent these aspects, since the bilinear model is rate-independent with a constant second stiffness.

To improve the deficiency of the bilinear model for HDRB, Sano and Pasquale (1995) have proposed a rate-independent model based on the Davienkov-Martine law to reproduce change of stiffness as well as of equivalent damping in a cyclic load for a wide range of strains. Kikuchi and Aiken (1997) have developed a rate-independent model for HDRB by employing both bilinear and Ramberg-Osgood models. More recently, Abe et al. (2004b)

have proposed a bi-directional elastoplastic model with hardening. These models account for some aspects of HDRB behavior, such as strain hardening and change in equivalent damping in sinusoidal loading. However, they are still rate-independent, and accordingly cannot reproduce change in stress response under different strain rates.

Few works have been reported in the development of the rate-dependent models of HDRBs. In the recent past, Hwang et al. (2002) have developed an analytical model to describe the damping and restoring forces of HDRBs. Both stiffness and damping coefficients are expressed in terms of a higher order polynomial function of the relative displacement and velocity of the bearing. All parameters of the model are determined from the cyclic loading tests of a particular bearing by utilizing the nonlinear least-square method. However, the physical basis of the mathematical model incorporating the rate-dependence to describe the stiffness and the damping coefficients is not clearly explained. Tsai et al. (2003) have developed a rate-dependent analytical model of HDRBs by extending the Wen's hysteretic model (Wen, 1976) in an incremental form. This model has described the restoring force in terms of the strain as well as velocity induced forces. However, the physical basis for separating the velocity induced forces from the other part of the total restoring force is not clearly stated in the model. Dall's Asta and Ragni (2006) have conducted cyclic shear tests and simple relaxation tests to identify the rate-dependent mechanical properties of HDRBs. On the basis of the experimental results, they have proposed a rate-dependent analytical model of HDRBs. The physical basis of the mathematical model describing the elasticity behavior of HDRBs is ambiguous.

Moreover, the mathematical model used for the viscosity behavior in loading and unloading cannot adequately describe for a general loading condition. Two other analytical models for HDRBs have been proposed by Hwang and Ku (1997); Hwang and Wang (1998); Koh and Kelly (1990) based on the results of the shaking table tests of seismically isolated bridge decks. In their proposed models, the fractional derivative of the relative displacement has replaced the relative velocity term of the equation of motion. These models are established using the fractional derivative of linear Kelvin and Maxwell models based on the sinusoidal test results. Hence, these models cannot reproduce the nonlinear mechanical behavior of HDRBs accurately.

A number of experimental and numerical works on high damping rubber (HDR) materials have been performed in the past (Amin et al., 2002, 2006; Hwang et al., 2002; Spathis and Kontou, 2008). These works show that the mechanical properties of HDR materials are dominated by the nonlinear rate-dependence including other inelastic behavior. Moreover, the different viscosity behavior in loading and unloading has been identified (Amin et al., 2002, 2006; Bergstrom and Boyce, 1998, 2000), and also incorporated in some analytical models through an Eyring type equation (Spathis and Kontou, 2008).

In order to develop a rate-dependent model suitable for seismic analysis of a bridge, the authors have conducted an experimental scheme comprised of multi-step relaxation (MSR) tests, cyclic shear (CS) tests, and simple relaxation (SR) tests. The objective of

MSR, CS, and SR tests was to identify the equilibrium response, instantaneous response, and nonlinear viscosity behavior of HDRBs, respectively. On the basis of the experimental results, a rate-dependent (elasto-viscoplastic) model is proposed. A structural configuration of the proposed model is presented in Fig.2 (a). The basic ideas are the additive decompositions of shear stress and strain as shown in Fig.2 (b). A parameter identification scheme is proposed to identify the parameters involved in different branches of the proposed model. In addition, an analytical scheme to identify nonlinear viscosity behavior of HDRBs in loading and unloading using the experimental data is discussed. The parameter identification scheme is successfully applied to the three specimens to show capability of the proposed model in reproducing the mechanical behavior of HDRBs. Finally, the adequacy of the proposed rheology model and parameter identification scheme is verified with experimental data obtained using sinusoidal loading history.

## **2. Mechanical behavior of the bearings**

In order to investigate the mechanical behavior of HDRBs, an experimental scheme was applied to three specimens referred to as HDR1, HDR2, and HDR3. Due to space limitation, experimental results of HDR2 are presented only; however, in discussion and comparative assessment other bearings' results (HDR1 and HDR3) are also included. The geometry and material properties of three specimens are given in Table 1 and Fig. 3. The dimensions of the test specimens are based on ISO standard (ISO, 2005).

Fig. 4 presents a flow diagram describing an outline for identification of parameters of the rheology model. The rheology model comprises of a number of parameters to be determined from experimental observations. In order to identify the model's parameters from the experimental data, MSR tests, CS tests, and SR tests were conducted in the proposed experimental scheme. MSR tests were conducted to identify the equilibrium response parameters of A, B, and S elements; CS tests to identify the instantaneous response parameter of C element, and a series of SR tests were carried out to identify the viscosity parameters of D element shown in Fig.2 (a). The equilibrium and instantaneous responses are theoretically defined as the responses under infinitely slow and fast loading rate, respectively. When the rate of loading is very slow i.e. the dashpot element D is not active as virtually no force is transmitted through it, and as a result A, B, and S elements are remaining, which constitutes the equilibrium response of the model. On the other hand, when the rate of loading is very high i.e. the dashpot element D is blocked since it has no sufficient time to deform and thereby A, B, C, and S elements are left over, which constructs the instantaneous response. The equilibrium and instantaneous responses thus obtained can be idealized as the elasto-plastic responses.

Due to presence of softening behavior in virgin rubber material, the first cycle of a stress-strain curve differs significantly from the shape of the subsequent cycles (Mullins, 1969). In order to remove the Mullins softening behavior from other inelastic phenomena, all specimens were preloaded before the actual tests. In the present study, the preloading was applied before MSR and SR tests only. The preloading was done by treating 11 cycles of

sinusoidal loading at 1.75 strain and 0.05 Hz until a stable state of the stress-strain response is achieved i.e. that no further softening occurs. The experimental results of MSR and SR tests are discussed in Section 2.1, 2.3 for virgin specimens, and in Section 4 for preloading specimens. Moreover, the effects of the preloading on equilibrium and viscosity parameters of the bearings are discussed in Section 4.

All specimens were tested under shear deformation with an average constant vertical compressive stress of 6 MPa. This mode of deformation is regarded as the most relevant one for application in base isolation. All tests were carried out with new specimens and using a computer-controlled servo hydraulic testing machine. The displacement was applied along the top edge of the specimen and the force response was measured by two load cells. All tests were carried out at around 23<sup>0</sup>C. All data were recorded using a personal computer. Throughout this paper, to express the experimental results, the average shear stress and shear strain are calculated using the following two equations

$$\gamma = \frac{u}{h}, \quad (1a)$$

$$\tau = \frac{F_h}{A}, \quad (1b)$$

where  $u$  and  $F_h$  denote the relative horizontal displacement and applied force, respectively;  $h$  stands for the total thickness of rubber layers and  $A$  is the area of the cross section.

### *2.1. Multi-step relaxation test (MSR test)*

Due to the inherent viscosity property in rubber material, it is practically impossible to identify the equilibrium response by applying infinitely slow loading rate. Hence, the MSR test was employed with the primary objective to identify the equilibrium response of HDRBs. Another objective of the MSR test was to investigate the viscosity property during loading and unloading, since the different strain rate sensitivity was clearly visible in loading and unloading of HDRBs (Fig.1). The similar approach was also employed by Amin et al. (2002); Bergstrom and Boyce (1998, 2000); Lion (1996, 1997) to identify the equilibrium response of rubber materials. The shear strain history applied in MSR test is presented in Fig. 5, where a number of relaxation periods of 20 min during which the applied strain is held constant are inserted in loading and unloading at a constant strain rate of 5.5/s.

Fig. 6(a) shows the resultant stress histories obtained in HDR2, in which the trend of convergence of the stress history to an almost constant state at the end of each relaxation period was demonstrated. The convergence of the stress responses is identified in an asymptotic sense (Lion, 1996). The shear stress-strain relationship in the equilibrium state can be obtained by connecting all the asymptotically converged stress values at each strain level as shown in Fig. 6(b). The difference of the stress values between loading and unloading at a particular shear strain level corresponds to the equilibrium hysteresis, which can be easily visualized in Fig.6 (b). This behavior may be attributed as an irreversible slip process between fillers in the rubber microstructures (Kilian et al., 1994;

Mullins, 1969), which is the resulting phenomenon of breaking of rubber-filler bonds (Bueche, 1960). Using the stress history data of Fig.6 (a), the over stress can be estimated by subtracting the equilibrium stress response from the current stress response at a particular strain level. While comparing between the over stresses in loading and unloading of Fig.6 (a), the over stress in loading is seen higher than in unloading. This may be associated with different viscosity behavior in loading and unloading. The similar phenomena with different magnitudes were depicted in HDR1 and HDR3 also.

## 2.2 *Cyclic shear test (CS test)*

The instantaneous response can be ideally obtained, when a viscous solid is loaded at an infinitely fast loading rate. From an experimental point of view, however, there exists an upper limit of the stroke rates for any displacement controlled loading machine. Hence, it is practically impossible to arrive at this loading rate in a viscous solid. In order to estimate the instantaneous response of HDRBs, a series of CS tests were conducted in this study. Three specimens were used in the experiments at different strain rates up to an absolute maximum strain of 1.75. The constant strain rates were maintained in each CS test within a range of 0.05/s - 5.5/s as shown in Fig.7.

Fig. 8 shows the rate-dependent shear stress-strain responses observed in CS tests along with the equilibrium responses obtained from MSR tests of HDR2. The shear stress responses observed in Fig. 8 are found to be nonlinear at all strain levels. A comparison of the stress responses at different strain rates indicates that the strong strain-rate

dependence exists in loading, whereas much weaker strain-rate dependence is observed in unloading. The different viscosity property in loading and unloading is attributed to this typical experimental observation. The similar phenomena were observed in other two bearings.

The basic strength elements of rubber are very long chain molecules, which are cross-linked with each other at some points to form a network (Trealor, 1975). Two types of linkages are occurred in rubber: physical linkages and chemical linkages. Due to the inherent properties of building up the physical and chemical linkages of rubber, the physical linkages are much weaker in stability and strength compared with the chemical linkages (Besdo and Ihlemann, 2003; Ihlemann, 1999). The physical linkages have small energy capacity, which are easily broken; however, the chemical linkages have higher energy capacity, which require external energy to be broken. In loading at a particular strain rate, some of the physical and chemical linkages are broken, however, in unloading at the same strain rate; the breaking up the physical linkages is more prominent than the chemical linkages. These phenomena may be associated with the different viscosity behavior in loading and unloading (see for example Fig.6 (a)).

Another comparison of hysteresis loops observed at different strain rates shows that the size of the hysteresis loops increases with the increase of strain rates; see for example Fig.8. While comparing among the three bearings, HDR2 demonstrates a bigger hysteresis loop in compared with the other two bearings. This typical behavior can be

attributed that HDR2 inherits relatively higher viscosity property than that in HDR1 and HDR3. To illustrate the rate-dependent hysteresis properties of HDRBs, the equilibrium hysteresis loop obtained from MSR test results was compared with the experimental results of CS tests as shown in Fig.8.

The strain-rate dependence during loading of HDR2 was illustrated in Fig.9. The shear stress response increased with increase of strain rates, however, at higher strain rates, a diminishing trend of the stress responses was observed indicating the neighboring state of the instantaneous response. Hence, the stress responses obtained at nearly 5.5/s can be considered as the neighboring state of the instantaneous response.

### 2.3. *Simple relaxation test (SR test)*

The multi-step relaxation test and cyclic shear tests described in Section 2.1 and 2.2 have illustrated the methods of estimating the equilibrium and instantaneous responses of HDRBs. The remaining part of the work is to investigate the viscosity property in HDRBs. To this end, a series of SR tests at different strain levels were carried out in this study. Fig. 10 shows the strain history of SR tests at three different strain levels of  $\gamma = 100, 150, \text{ and } 175\%$  with a strain rate of 5.5/s. The stress histories obtained in SR tests of HDR2 are presented in Fig.11. A rapid stress relaxation was displayed in the first few minutes; after while it approached asymptotically towards a converged state of responses (Fig.11). The amount of stress relaxation in loading and unloading of HDR2 was found much higher than those of HDR1 and HDR3. The larger stress relaxation in HDR2 has

the direct conformity with the results of CS tests (see for example Fig.8). The stress response obtained at the end of the relaxation can be regarded as the equilibrium stress response. The deformation mechanisms associated with relaxation are related to the long chain molecular structure of the rubber. In the relaxation test, the initial sudden strain occurs more rapidly than the accumulation capacity of molecular structure of rubber. However, with the passage of time the molecules again rotate and unwind so that less stress is needed to maintain the same strain level.

Fig.13 shows the stress histories obtained under two different strain histories shown in Fig.12. Although the maximum over stresses are different depending on the strain rates in loading and unloading regimes, the relaxation curves are almost identical to each other (Fig.13). It can be concluded that the relaxation behavior is not dependent on the maximum over stress.

### **3. Rheology model**

#### *3.1. General motivation and model structure*

In this paper, a set of experimental data as discussed in Section 2 is utilized to design the proposed rheology model of HDRBs. The mechanical behavior of HDRBs exhibits the rate-dependent response accompanied by rate-independent responses. These mechanical responses motivate to design the basic structures of the elasto-viscoplastic rheology model as presented in Fig.2.

In this model, the total stress is decomposed into three branches as shown in Fig. 2:

$$\tau = \tau_{ep}(\gamma_a) + \tau_{ee}(\gamma) + \tau_{oe}(\gamma_c), \quad (2)$$

where  $\tau_{ep}$  is the stress in the first branch composed of a spring (Element A) and a slider (Element S);  $\tau_{ee}$  denotes the stress in the second branch with a spring (Element B);  $\tau_{oe}$  does that in the third branch composed of a spring (Element C) and a dashpot (Element D). The first and second branches represent the rate-independent elasto-plastic behavior, while the third branch introduces the rate-dependent behavior.

In addition to the stress decomposition, the strain is decomposed into two different ways:

$$\gamma = \gamma_a + \gamma_s = \gamma_c + \gamma_d, \quad (3)$$

where  $\gamma_a$  and  $\gamma_c$  stand for the strains in Element A and C, respectively;  $\gamma_s$  and  $\gamma_d$  are the strains for the slider (Element S) and the dashpot (Element D), respectively. In the subsequent sections, rate-independent part of the rheology model will be discussed followed by parameter identification for rate-dependent part.

### 3.2. *Equilibrium hysteresis*

From MSR test data, an equilibrium hysteresis loop with strain hardening is visible in each bearing; see for example Fig.6 (b) for HDR2). This equilibrium hysteresis loop can be suitably reproduced by combining the nonlinear elastic response with ideal elasto-plastic response.

Accordingly, spring A is assumed as linear spring:

$$\tau_{ep} = C_1 \gamma_a, \quad (4)$$

where  $C_1$  is a spring constant for spring A.

The friction slider will be active, when the stress level in the slider reaches a critical shear stress  $\tau_{cr}$  i.e.

$$\begin{cases} \dot{\gamma}_s \neq 0 & \text{for } |\tau_{ep}| = \tau_{cr} \\ \dot{\gamma}_s = 0 & \text{for } |\tau_{ep}| < \tau_{cr} \end{cases} \quad (5)$$

In order to express the hardening at higher strain levels, a nonlinear spring is used for element B:

$$\tau_{ee} = C_2\gamma + C_3|\gamma|^m \text{sgn}(\gamma) \quad (6)$$

where  $C_2$ ,  $C_3$ , and  $m$  ( $m > 1$ ) are constants with

$$\text{sgn}(x) = \begin{cases} +1 & : x > 0 \\ 0 & : x = 0 \\ -1 & : x < 0 \end{cases} \quad (7)$$

Now, let us identify the parameters for the rate-independent equilibrium response. The critical shear stress,  $\tau_{cr}$  is determined by using the equilibrium hysteresis loop; see for example Fig.6 (b). The difference between loading and unloading stresses in the equilibrium hysteresis loop at each strain level corresponds to  $2\tau_{cr}$ . Accordingly,  $\tau_{cr}$  can be determined from the half of the arithmetic average values of the stress differences. Next, the parameter  $C_1$  corresponding to the initial stiffness can be determined by fitting the initial part as well as the switching parts from loading and unloading in the equilibrium hysteresis loop. Finally, the parameters for the nonlinear spring (Element B) will be identified. The subtraction of the stress  $\tau_{ep}$  of Eq.(4) from the equilibrium stress obtained from MSR test gives the stress  $\tau_{ee}$  corresponding to Eq.(6). By using the standard least square method, parameters  $C_2$ ,  $C_3$ , and  $m$  are determined. The obtained critical stresses

and the equilibrium response parameters  $C_2$ ,  $C_3$ , and  $m$  for all bearings are given in Table 2. The equilibrium responses obtained using the proposed model with the identified parameters, and the experimental results are presented in Fig. 14.

### 3.3. *Instantaneous response*

At the instantaneous state, the structure of the rheology model can be reduced into the same model without the dashpot element (Element D), because the dashpot is fixed ( $\dot{\gamma}_d = 0$ ) owing to infinitely high strain rate loading. Consequently, the instantaneous response of the rheology model can be obtained by adding  $\tau_{oe}$  without Element D and the responses obtained from the other two branches. From CS test results, a diminishing trend of the stress responses with increasing strain rates was observed in all bearings; see for example Fig.9 (reply of the comment is attached). Hence, an instantaneous stress-strain curve can be obtained at the neighborhood of the stress-strain curve at a strain rate of 5.5/s, which is the maximum strain rate in the current CS tests. The instantaneous stress-strain curve, and accordingly the spring C seems to be nonlinear even in loading regime (Fig.8). For simplicity, however, a linear spring model is employed for Element C:

$$\tau_{oe} = C_4 \gamma_c, \quad (8)$$

where  $C_4$  is the spring constant for Element C.

The parameter  $C_4$  is determined so that the instantaneous stress-strain curve calculated from the rheology model ( $\tau = \tau_{ee} + \tau_{ep} + \tau_{oe}$  (without the dashpot element)) can envelop the stress-strain curves obtained from CS tests. Fig. 15 shows comparison between

the instantaneous stress-strain curve from the rheology model and those from CS tests at different strain rates up to 5.5/s in loading regime of HDR2. The obtained parameters  $C_4$  for all bearings are listed in Table 2.

### 3.4. *Nonlinear viscosity*

This section describes the procedure to identify the constitutive relationship of the dashpot (Element D) in the rheology model. To this end, the experimental results obtained from MSR and SR tests are analyzed to procure the relationship between the over stress  $\tau_{oe}$  and the dashpot strain rate  $\dot{\gamma}_d$ . A schematic diagram to identify  $\tau_{oe} - \dot{\gamma}_d$  relationship is presented in Fig. 16. From the stress relaxation results of MSR and SR tests, we have the time histories of the total stress  $\tau$  and the total strain  $\gamma$ . Assuming that the asymptotic stress response at the end of each relaxation period is the equilibrium stress  $\tau_{eq}$  at a particular strain level, the over stress history in each relaxation period is obtained by subtracting the equilibrium stress from the total stress. Then, the time history of the elastic strain for Element C is calculated from  $\gamma_c = \tau_{oe}/C_4$  in Eq.(8), and consequently the time history of the dashpot strain can be determined as  $\gamma_d = \gamma - \gamma_c$  using Eq. (3). The history of the dashpot strain has been evaluated using a special scheme before taking the time derivative of experimental data, which usually contain scattering due to noise. In this regard, a moving averaging technique is adopted before taking the time derivative of the experimental data (Wolfram, 2005).

Fig. 17 shows the relationships between the over stress and the dashpot strain rates obtained from SR test results. In SR tests, the total strains were assigned from 0 to 100, 150, 175% for loading, and then the strains were reduced to 0 for unloading; see Fig. 10 for the strain history. The values in the legend stand for the total strain in respective relaxation processes, and 100, 150, 175% correspond to relaxation process after loading, and 0% after unloading. This figure demonstrates nonlinear dependence of the over stress on the dashpot strain rate. Since the gradient of  $\tau_{oe} - \dot{\gamma}_d$  curves represents the viscosity, the viscosity decreases with increasing dashpot strain rates. Furthermore, it is found that these relationships depend on the strain levels in the relaxation tests after loading; i.e. the over stress, and accordingly the viscosity, increases with increasing the total strain. The same tendency is also visible for MSR test data in Fig.18. In this figure, the positive over stress indicates relaxation after loading, while the negative one does after unloading. It should be noted that the dependence of the over stress on the total strain level after unloading is not noticed significant as that observed after loading; see for example Fig.18.

In order to describe the nonlinear viscosity of the dashpot, first we have to distinguish loading and unloading with respect to the dashpot. We define the loading and unloading condition for the dashpot as follows:

$$\frac{d}{dt}|\dot{\gamma}_d| > 0 \text{ for loading,}$$

$$\frac{d}{dt}|\dot{\gamma}_d| < 0 \text{ for unloading.}$$

This loading-unloading condition is identical with

$$\tau_{oe}\dot{\gamma}_d > 0 \text{ for loading,}$$

$$\tau_{oe}\dot{\gamma}_d < 0 \text{ for unloading.}$$

Based on the  $\tau_{oe} - \dot{\gamma}_d$  relationships obtained from MSR and SR test data shown in Figs.17 and 18, the dashpot's constitutive model is expressed by

$$\tau_{oe} = A_l \exp(q|\gamma|) \operatorname{sgn}(\dot{\gamma}_d) \left| \frac{\dot{\gamma}_d}{\dot{\gamma}_o} \right|^n \text{ for loading,} \quad (9a)$$

$$\tau_{oe} = A_u \operatorname{sgn}(\dot{\gamma}_d) \left| \frac{\dot{\gamma}_d}{\dot{\gamma}_o} \right|^n \text{ for unloading,} \quad (9b)$$

where  $\dot{\gamma}_o = 1 \text{ (sec}^{-1}\text{)}$  is a reference strain rate of the dashpot;  $A_l$ ,  $A_u$ ,  $q$  and  $n$  are constants for nonlinear viscosity.

In MSR and SR tests, the loading/unloading condition changes clearly (e.g. Figs. 5 and 10). However, under general loading/unloading histories, the loading/unloading condition may change gradually. To avoid abrupt change in viscosity due to a shift in the loading and unloading condition, a smooth function is introduced into the over stress expression, and Eq.(9) can be rewritten in a more compact form

$$\tau_{oe} = A \left| \frac{\dot{\gamma}_d}{\dot{\gamma}_o} \right|^n \operatorname{sgn}(\dot{\gamma}_d) \quad (10a)$$

with

$$A = \frac{1}{2} (A_l \exp(q|\gamma|) + A_u) + \frac{1}{2} (A_l \exp(q|\gamma|) - A_u) \tanh(\xi \tau_{oe} \dot{\gamma}_d), \quad (10b)$$

where  $\zeta$  is the smoothing parameter to switch viscosity between loading and unloading. Now, in the subsequent paragraphs, the procedure for determining the viscosity constants ( $A_l$ ,  $A_u$ ,  $q$  and  $n$ ) will be discussed followed by the smoothing parameter ( $\zeta$ ).

Using the strain histories of the SR tests at different strain levels (Fig.10), the over stress-dashpot strain rate relationships are determined (Fig. 17), which correspond to Eq.9 (a) and (b) for loading and unloading, respectively. A standard method of nonlinear regression analysis is employed independently in Eq. 9(a) and (b) to identify the viscosity constants for loading and unloading, respectively. As motivated by the relationships of the over stress-dashpot strain rates obtained in the SR test results (e.g.Fig.17), the value of  $n$  is kept the same in loading and unloading. The nonlinear viscosity parameters obtained in this way are presented in Table 3. Fig. 17 presents the overstress-dashpot strain rate relationships obtained using the proposed model and the SR test results.

A sinusoidal loading history is utilized to determine the smoothing parameter of the model. The sinusoidal loading history corresponds to a horizontal displacement history applied at the top of the bearing at a frequency of 0.5 Hz and the absolute strain amplitude of 1.75(reply of the comment is attached). An optimization method based on the Gauss-Newton algorithm (Venkataraman, 2002) is employed in Eq.(10) to determine the smoothing parameter. The optimization problem is mathematically defined as minimizing the error function presented as

$$\text{Minimize} \left\{ E(\zeta, t) = \sum_{n=1}^N (\tau_{exp,n} - \tau_{m,n})^2 \right\} \quad (11)$$

where  $N$  represents the number of data points of interest,  $\tau_{exp,n}$  and  $\tau_{m,n}$  correspond to the shear stress responses at any time instant  $t_n$  obtained from the experiment and the model, respectively, and  $\zeta$  stands for the parameter to be identified. Using a standard method, the error function shown in Eq. (11) is minimized and the corresponding values of  $\zeta$  are determined for the specified loading condition. The values of  $\zeta$  for the three bearings are presented in Table 3.

#### 4. Numerical simulations and discussions

The experimental results presented in Section 2 revealed the viscosity induced rate-dependent behavior along with other inelastic properties of HDR bearings. Section 3 was devoted to develop the rheology model along with a scheme for determining the parameters utilizing the experimentally observed behavior of HDR bearings. In this Section, the rheology model is used to simulate the experimental results obtained using the sinusoidal loading data. In order to remove the Mullin's softening effect (Mullins, 1969) of the HDR material, the 4<sup>th</sup> cycle shear stress-strain responses are used in the simulation. The elasticity and viscosity parameters used for this purpose are presented in Tables 2 and 4. The equilibrium responses do not depend on the specimens' condition, i.e. whether it is virgin or preloading specimen, which is typically displayed in Fig.19 for HDR2. From this figure, it is clearly seen that the equilibrium responses in both conditions follow the similar shape. Considering this fact, the same equilibrium response

parameters have been used for simulating the 4<sup>th</sup> cycle stress responses. To illustrate the effect of the preloading on the viscosity behavior of the bearings, the  $\tau_{oe} - \dot{\gamma}_d$  relationships obtained from SR test data with a strain level of 1.75 using the virgin and the preloading specimens are typically presented in Fig. 20 for HDR2. The similar behavior was also observed in other two bearings (HDR1 and HDR3). From these figures, it has been clearly observed that the shapes of the  $\tau_{oe} - \dot{\gamma}_d$  curves in both virgin and preloading specimens during loading and unloading remain similar, i.e. the values of  $q$  and  $n$  can be kept the same in both conditions. However, the magnitude of the over stress in the virgin specimens was seen larger than that in the preloading specimens at corresponding dashpot strain rates during loading/unloading. The same tendency has been also observed at other strain levels. Taking this fact into account, the values of  $A_l$  and  $A_u$  are modified in the simulation as shown in Table 4. In this simulation, the sinusoidal loading data, a different loading history from that used in the parameter identification, is used to illustrate capability of the proposed model in predicting the mechanical behavior of HDR bearings. Figs. 21 (a) to (c) present the simulated stress responses of sinusoidal loading experiments for the three bearings. The results are comparable very closely with the experiments in predicting the stress responses in loading and unloading. Furthermore, a smooth shifting of the stress response from the loading to unloading and vice-versa is also predicted well.

## 5. Concluding remarks

An experimental scheme was performed in order to investigate the mechanical behavior of HDR bearings under horizontal cyclic shear deformation with a constant vertical compressive load. The equilibrium response of the bearings can be asymptotically identified from MSR test results. The neighborhood of the instantaneous response of the bearings can be approximated by conducting a series of CS tests at different strain rates. These two experimental results represent the rate-independent response of the bearings. The rate-dependent behavior of the bearings can be obtained from SR and MSR tests results. The different rate-dependence is also observed in loading and unloading of MSR tests. On the basis of experimental results, an elasto-viscoplastic model capable of describing the mechanical behavior in the range of interest for seismic applications (JRA, 1996 and 2002) is developed. The model can adequately represent the equilibrium response of the bearings. However, due to a linear assumption in deriving the stress-strain relationship of the over stress (Eq.(8)), the instantaneous response could not be closely predicted by the model. After the equilibrium and instantaneous response parameters of the bearings are estimated, the viscosity parameters are identified utilizing the SR test results. A comparison carried out between the simulations and the experimental results shows that the proposed model is well capable of predicting the nonlinear viscosity in loading and unloading of the HDR bearings in addition to other inelastic behavior. This permits overcoming limitations of the previous seismic analysis models based on the elasto-plastic hysteresis behavior. However, the present work has suggested for

development of a rheology model of HDR bearings incorporating the Mullins softening behavior. It is the current interest of the authors to address this aspect.

### **Acknowledgements**

The experimental works were conducted by utilizing the laboratory facilities and bearings-specimens provided by Bridgestone Company, Tokai Rubber Industry and Yokohama Rubber Company, Japan. The authors indeed gratefully acknowledge the kind cooperation extended by them. The authors also sincerely acknowledge the funding provided by the Japanese Ministry of Education, Science, Sports and Culture (MEXT) as Grant-in-Aid for scientific research to carry out this research work.

## References

- Abe, M., Yoshida, J., Fujino, Y., 2004a. Multiaxial behaviors of laminated rubber bearings and their modeling. I: Experimental study. *Journal of Structural Engineering* 130, 1119-1132.
- Abe, M., Yoshida, J., Fujino, Y., 2004b. Multiaxial behaviors of laminated rubber bearings and their modeling. I: Modeling. *Journal of Structural Engineering* 130, 1133-1144.
- American Association of State Highways and Transportation Officials (AASHTO), 2000. *Guide specification for seismic isolation design*, 2/e.
- Amin., A.F.M.S., Alam, M.S., Okui, Y., 2002. An improved hyperelasticity relation in modeling viscoelasticity response of natural and high damping rubbers in compression: experiments, parameter identification and numerical verification. *Mechanics of Materials* 34, 75-95.
- Amin., A.F.M.S., Lion, A., Sekita, S., Okui, Y., 2006. Nonlinear dependence of viscosity in modeling the rate-dependent response of natural and high damping rubbers in compression and shear: experimental identification and numerical verification. *International Journal of Plasticity* 22, 1610-1657.
- Bergstrom, J. S., Boyce, M. C., 1998. Constitutive modeling of the large strain time-dependent behavior of elastomers. *Journal of the Mechanics and Physics of Solids* 46, 931-954.
- Bergstrom, J. S., Boyce, M. C., 2000. Large strain time-dependent behavior of filled elastomers. *Mechanics of Materials* 32, 627-644.

Besdo, D., Ihlemann, J., 2003. Properties of rubber like materials under large deformations explained by self-organizing linkage patterns. *International Journal of Plasticity* 19, 1001-1018.

Bueche, F., 1960. Molecular basis for the Mullins effect. *Journal of Applied Polymer Science* 4, 107-114.

Dall'Asta, A., Ragni, L., 2006. Experimental tests and analytical model of high damping rubber dissipating devices. *Engineering Structures* 28, 1874-1884.

Hwang, J. S., Ku, S.W., 1997. Analytical modeling of high damping rubber bearings. *Journal of Structural Engineering* 123, 1029-1036.

Hwang, J.S., Wang, J.C., 1998. Seismic response prediction of HDR bearings using fractional derivatives Maxwell model. *Engineering Structures* 20, 849-856.

Hwang, J.S., Wu, J. D., Pan, T. C., Yang, G., 2002. A mathematical hysteretic model for elastomeric isolation bearings. *Earthquake Engineering and Structural Dynamics* 31, 771-789.

International Organization of Standardization (ISO), 2005. *Elastomeric seismic-protection isolators, Part 1: Test methods*.

Ihlemann, J., 1999. Modeling of inelastic rubber behavior under large deformations based on self-organizing linkage patterns. *Proceedings of the First European Conference on Constitutive Models for Rubber*. Vienna, Austria. A.A. Balkema Publishers, London, UK.

Japan Road Association, 1996. *Specifications for highway bridges, Part V: Seismic design*.

Japan Road Association, 2002. Specifications for highway bridges, Part V: Seismic design.

Kilian, H.G., Strauss, M., Hamm, W., 1994. Universal properties in filler-loaded rubbers. *Rubber Chemistry and Technology* 67, 1-16.

Kikuchi, M., Aiken, I.D., 1997. An analytical hysteresis model for elastomeric seismic isolation bearings. *Earthquake Engineering and Structural Dynamics* 26, 215-231.

Koh, C.G., Kelly, J.M., 1990. Application of fractional derivatives to seismic analysis of base isolated models. *Earthquake Engineering and Structural Dynamics* 19, 229-241.

Lion, A., 1996. A constitutive model for carbon black filled rubber: Experimental investigations and mathematical representation. *Continuum Mechanics and Thermodynamics* 8, 153-169.

Lion, A., 1997. A physically based method to represent the thermo-mechanical behavior of elastomers. *Acta Mechanica* 123, 1-25.

Mullins, L., 1969. Softening of rubber by deformation. *Rubber Chemistry and Technology* 42, 339-362.

Sano, T., Di Pasquale, G., 1995. A constitutive model for high damping rubber bearings. *Journal of Pressure Vessel Technology* 117, 53-57.

Salomon, O., Oller, S., Barbat, A., 1999. Finite element analysis of base isolated buildings subjected to earthquake loads. *International Journal for Numerical Methods in Engineering* 46, 1741-1761.

Skinner, R.I., Robinson, W.H., McVerry, G.H., 1993. An introduction to seismic isolation. DSIR Physical Science, Wellington, New Zealand.

Spathis, G., Kontou, E., 2008. Modeling of nonlinear viscoelasticity at large deformations. *Journal of Material Science* 43, 2046-2052

Treloar, L R.G., 1975. *The Physics of Rubber Elasticity*, 3/e, Oxford Univ. Press.

Tsai, C.S., Chiang, Tsu-Cheng, Chen, Bo-Jen, Lin, Shih-Bin, 2003. An advanced analytical model for high damping rubber bearings. *Earthquake Engineering and Structural Dynamics* 32, 1373-1387

Venkataraman, P., 2002. *Applied optimization with Matlab programming*. John Wiley and Sons, New York.

Wen, Y.K. 1976. Method for random vibration of hysteretic systems. *Journal of Engineering Mechanics*, 102, 249-263.

Wolfram Research Inc. 2005. *Mathematica Version 5.2*, USA.

## FIGURE CAPTIONS

Figure 1. Typical shear stress-strain responses of HDRB from CS tests. Shear stress ( $\tau$ ) is the horizontal force ( $F_h$ ) applied at the top of the bearing divided by the area ( $A$ ) of the cross section and the shear strain ( $\gamma$ ) is the relative horizontal displacement between top and bottom of the bearing divided by the total thickness of the rubber layers.

Figure 2. Rheology model. Superimposed stress response  $\tau = \tau_{ep} + \tau_{ee} + \tau_{oe}$ , where  $\tau_{ep}$ ,  $\tau_{ee}$ , and  $\tau_{oe}$  represent the rate independent elasto-plastic stress, nonlinear elastic stress and the nonlinear viscoelastic overstress, respectively.

Figure 3. Size of laminated rubber bearing used in experiment (a) Plan and side view [mm] (b) Detail of side view [mm]

Figure 4. Flow diagram of parameter identification of the rheology model; “S”, “A”, “B”, “C”, and “D” refer to elements in Fig.2.

Figure 5. Applied strain histories in MSR test; a shear strain rate of 5.5/s was maintained at each strain step.

Figure 6. Typical MSR test results (a) stress history (b) equilibrium stress response; equilibrium response at a particular strain level shows the response, which is asymptotically obtained from the shear stress histories of MSR test.

Figure 7. Strain histories applied in CS tests under shear strain rates of 5.5, 1.5, 0.5, and 0.05 1/s

Figure 8. Typical shear stress-strain relationships obtained from CS tests at different strain rates; equilibrium response is also presented for clear comparison.

Figure 9. Typical shear stress response as a function of strain rates recorded from CS tests at different strain levels.

Figure 10. Strain histories applied in SR tests at different strain levels; strain rate for loading and unloading regimes was assigned to 5.5/s. For clear illustration, the strain histories have been separated by 50 sec to each other.

Figure 11. Typical shear stress histories obtained from SR tests at different strain levels. For clear illustration, the stress histories have been separated by 50 sec to each other.

Figure 12. Strain rates applied in SR tests at strain level 1.75.

Figure 13. Typical strain rate dependency of stress relaxation obtained from SR tests; strain level in both strain rates was maintained at 175% after loading and 0% after unloading. For clear illustration, the stress histories have been separated by 50 sec to each other.

Figure 14. Identification of equilibrium response parameters; the experimental results are obtained from MSR tests in asymptotic sense and the model results are determined using  $\tau = \tau_{ee} + \tau_{ep}$  with parameters given in Table 2.

Figure 15. Identification of instantaneous response parameters; the instantaneous response is determined using the model  $\tau = \tau_{ee} + \tau_{ep} + \tau_{oe}$  (without dashpot element D) and the experimental results represented by different lines are obtained from CS tests at four strain rates of 0.05, 0.5, 1.5, and 5.5 /sec in loading regimes.

Figure 16. Schematic diagram to determine the analytical relationship between the over stress and the dashpot strain rates.

Figure 17. Identification of viscosity parameters; the model results represented by solid lines are obtained by  $\tau = \tau_{oe}$  with parameters given in Table 3 and the relations between  $\tau_{oe} - \dot{\gamma}_d$  as calculated from SR test data are shown by points. The values in the legend stand for the total strain in respective relaxation processes, and 100,150, 175% correspond to relaxation processes after loading, and 0% after unloading. The strain histories are given in Fig.10.

Figure 18. Typical overstress-dashpot strain rate relations obtained from MSR test results in loading and unloading regimes at different strain levels; the values in the legend stand for the total strain in respective relaxation processes, and 50,100, 150% correspond to relaxation processes after loading and unloading.

Figure 19. Typical equilibrium hysteresis obtained from MSR tests using the virgin and preloading specimens; filled circular points indicate the equilibrium response using the preloading specimens whereas the open triangular points do for the virgin specimens.

Figure 20. Effect of the preloading on the viscosity behavior of the bearings; filled circular points indicate the relations between  $\tau_{oe} - \dot{\gamma}_d$  as calculated from SR test data using the preloading specimens whereas the star points do for the virgin specimens.

Figure 21. Numerical simulations of sinusoidal loading data (a) HDR1, (b) HDR2, and (c) HDR3; the 4<sup>th</sup> cycle stress responses are considered in the simulations to simply remove the Mullins softening effect.

Table 1

Dimension and material properties of HDR bearings

Particulars	Specifications
Cross-section (mm <sup>2</sup> )	240X240
Number of rubber layers	6
Thickness of one rubber layer (mm)	5
Thickness of one steel layer (mm)	2.3
Nominal shear modulus (MPa)	1.2

Table 2

Elasticity parameters of HDR bearings

Type of rubber bearing	C <sub>1</sub> (MPa)	$\tau_{cr}$ (MPa)	C <sub>2</sub> (MPa)	C <sub>3</sub> (MPa)	C <sub>4</sub> (MPa)	m
HDR1	2.40	0.205	0.535	0.00177	2.80	8.18
HDR2	2.50	0.247	0.653	0.00620	3.25	6.62
HDR3	2.10	0.296	0.595	0.00241	2.65	7.42

Table 3

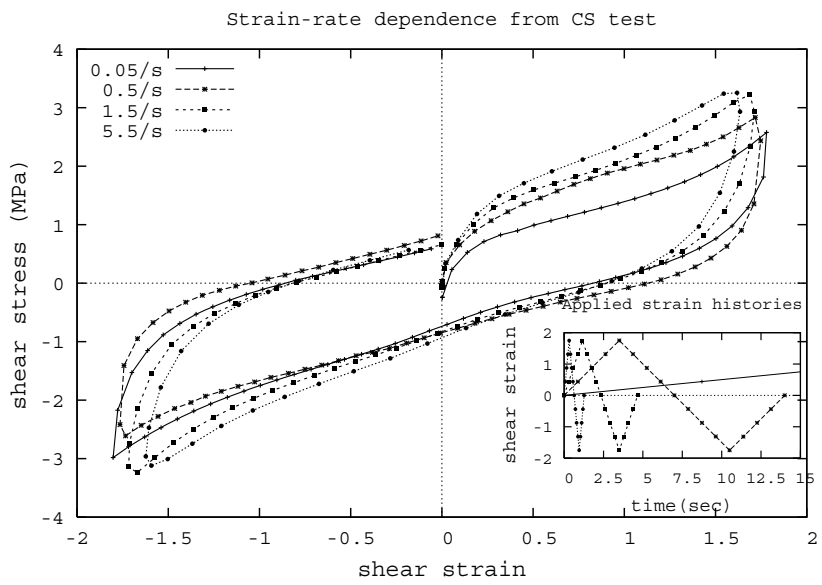
Viscosity and smoothing parameters of HDR bearings

Type of rubber material	$A_l$ (MPa)	$A_u$ (MPa)	q	n	$\xi$
HDR1	0.58	0.75	0.53	0.20	1.22
HDR2	1.12	1.02	0.34	0.22	1.25
HDR3	0.86	0.85	0.35	0.21	1.24

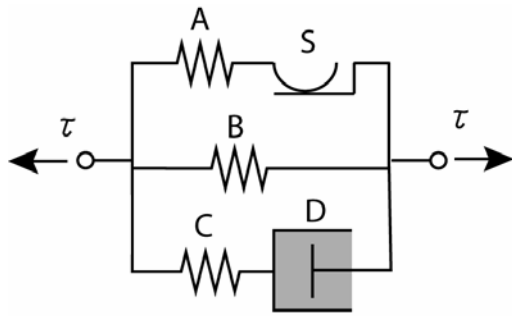
Table 4:

Viscosity and smoothing parameter used in the simulation of HDR bearings

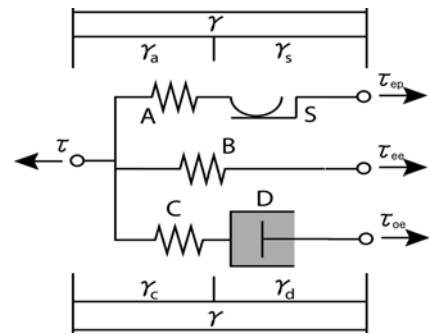
Type of rubber material	$A_l$ (MPa)	$A_u$ (MPa)	q	n	$\xi$
HDR1	0.30	0.20	0.53	0.20	1.22
HDR2	0.35	0.27	0.34	0.22	1.25
HDR3	0.40	0.24	0.35	0.21	1.24



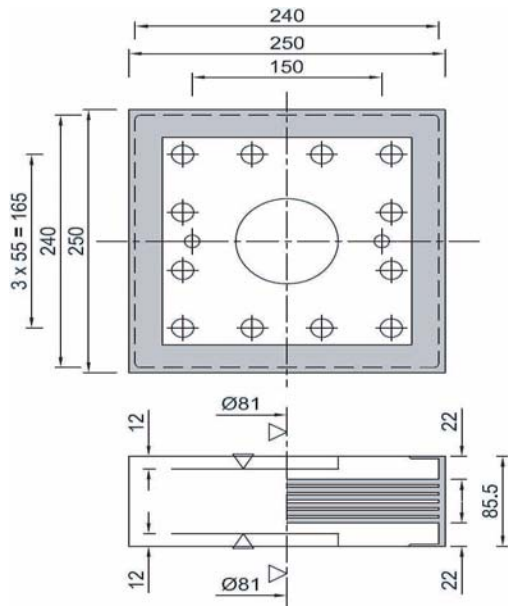
**[Figure 1]**



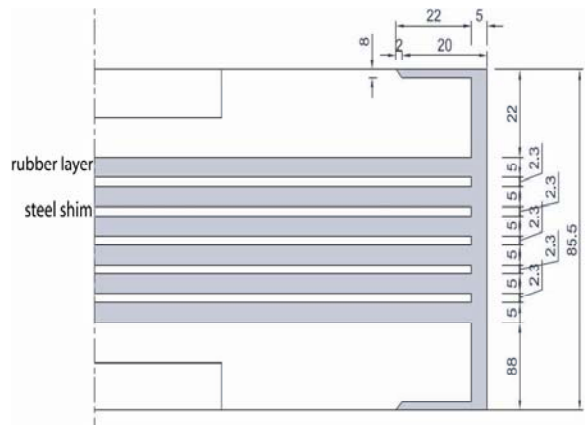
[Figure 2a]



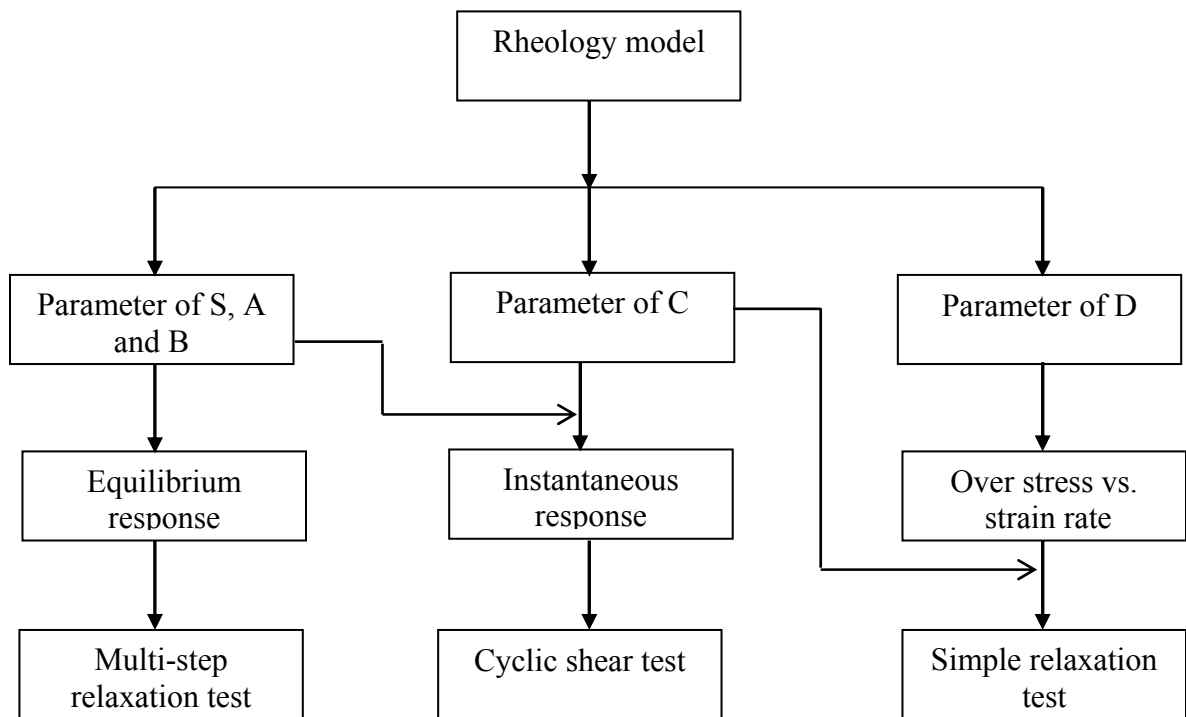
[Figure 2b]



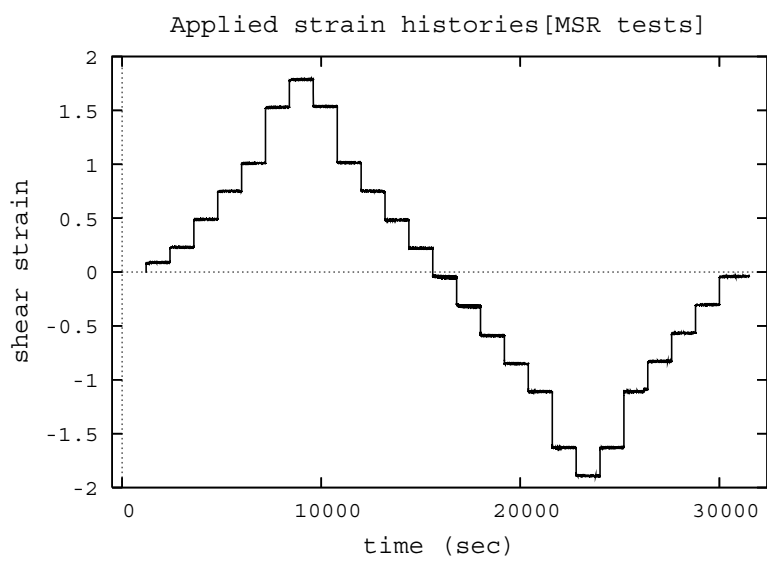
[Figure 3a]



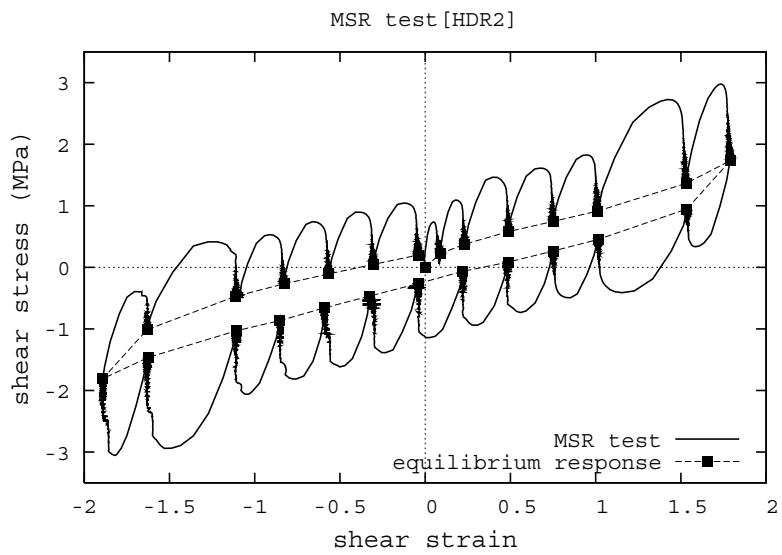
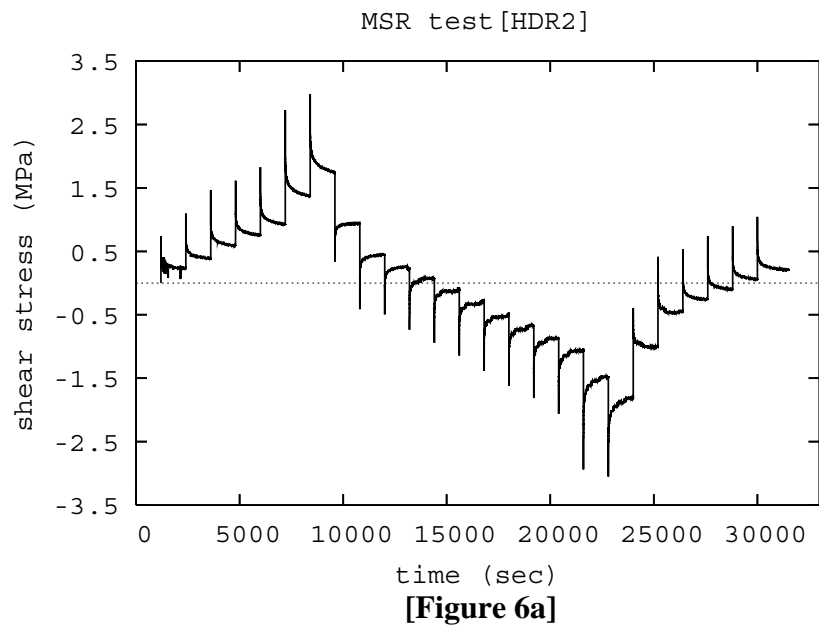
[Figure 3b]

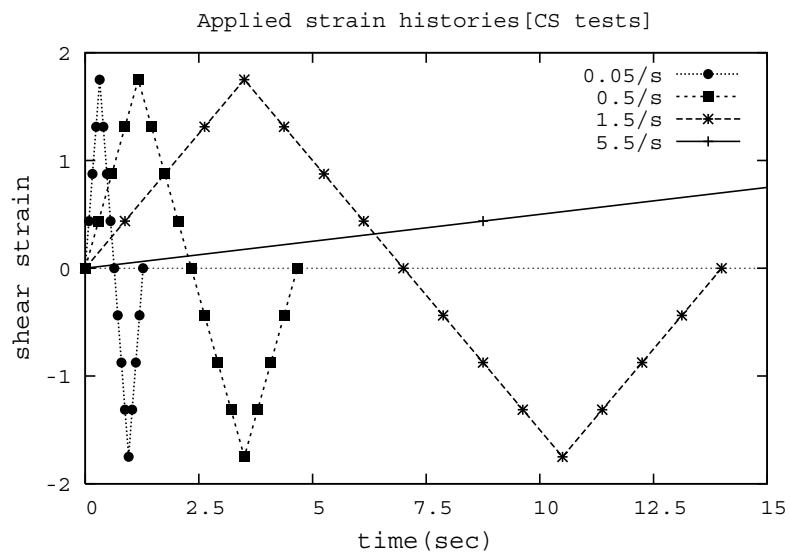


[Figure 4]

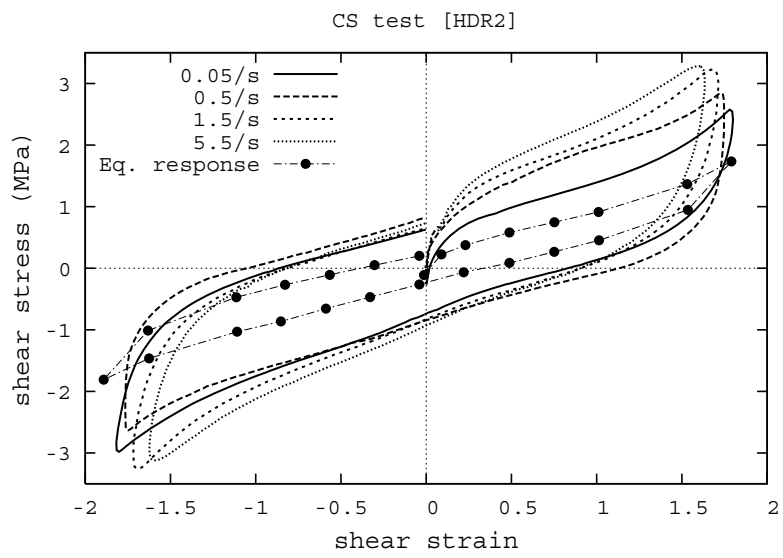


**[Figure 5]**

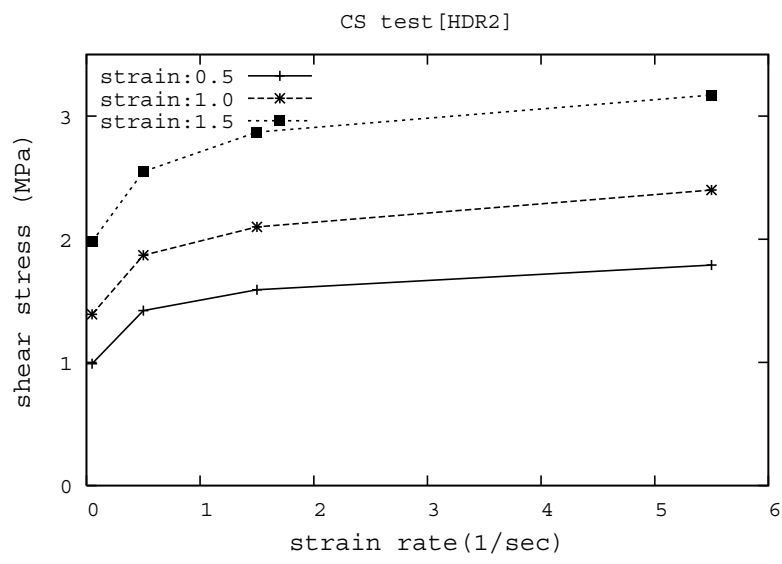




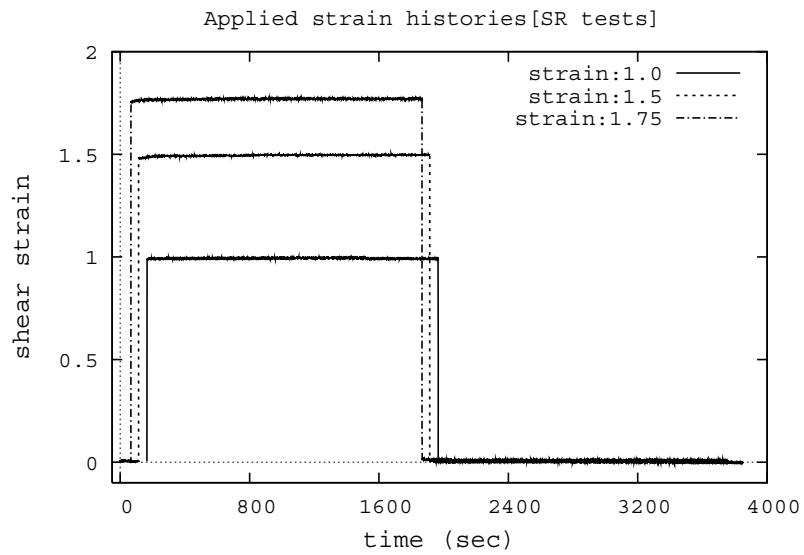
[Figure 7]



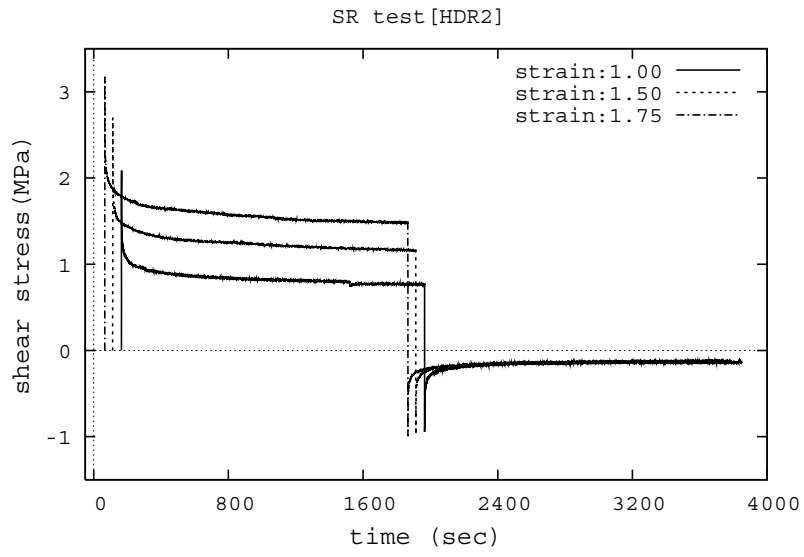
**[Figure 8]**



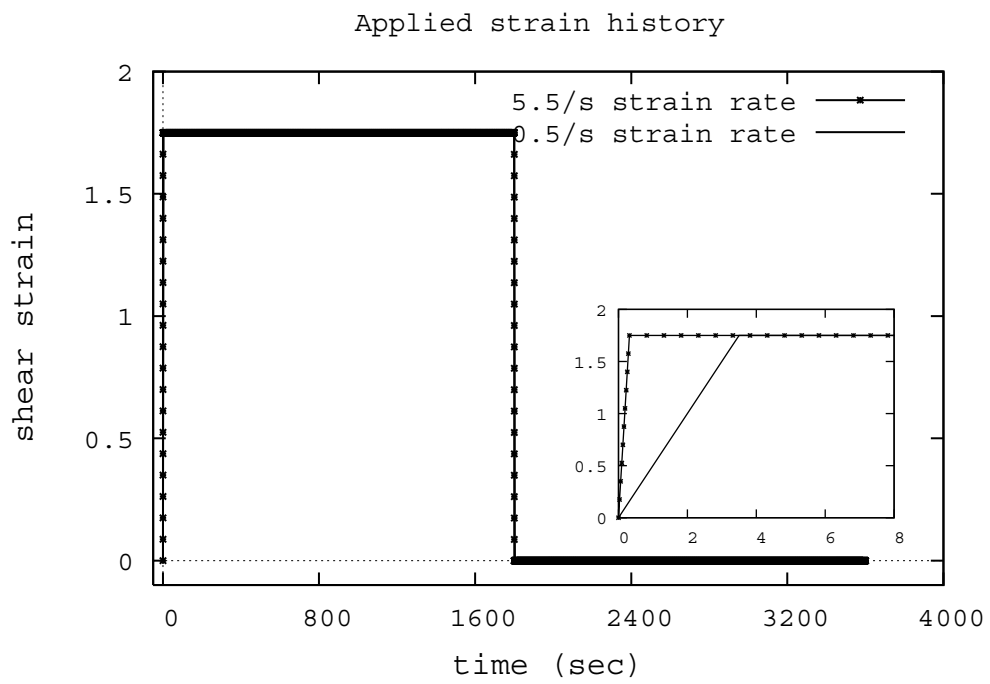
[Figure 9]



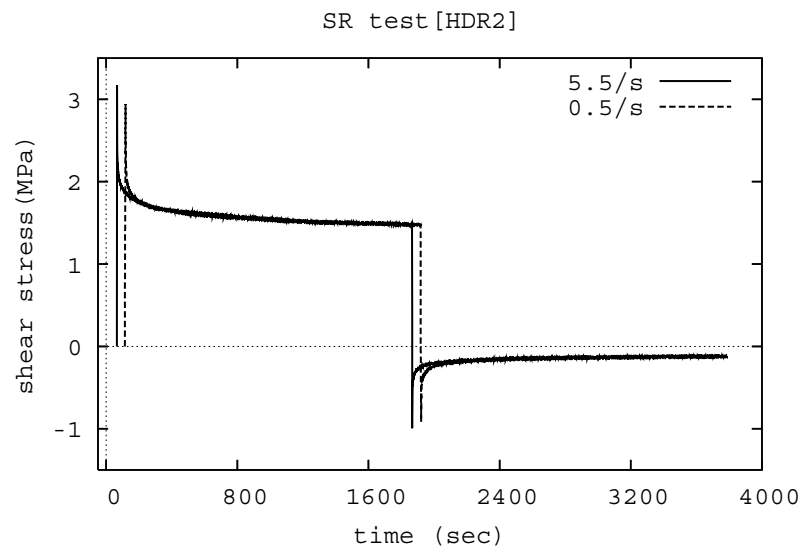
**[Figure 10]**



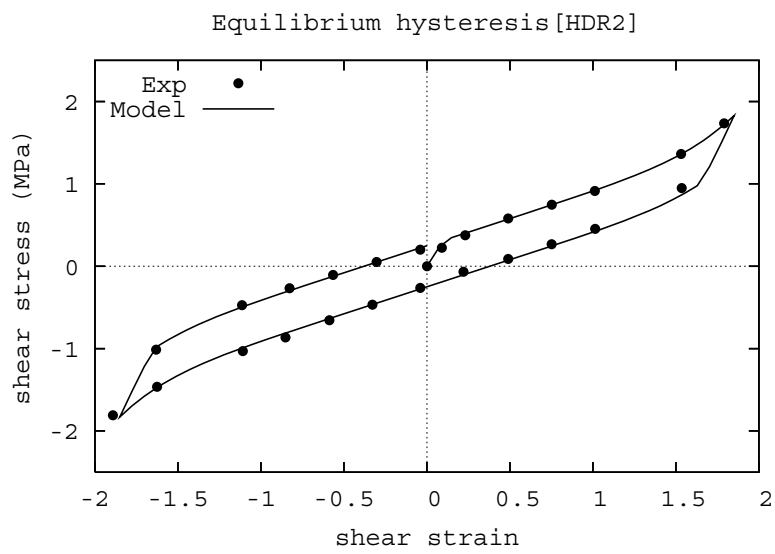
**[Figure 11]**



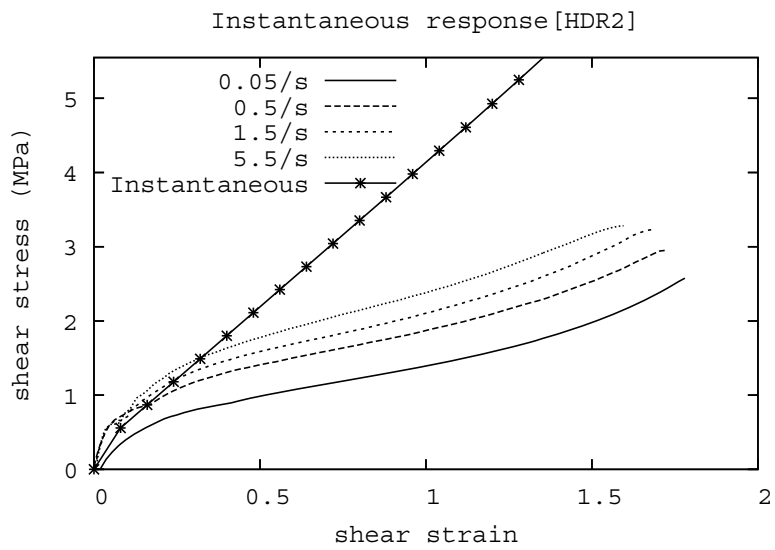
[Figure 12]



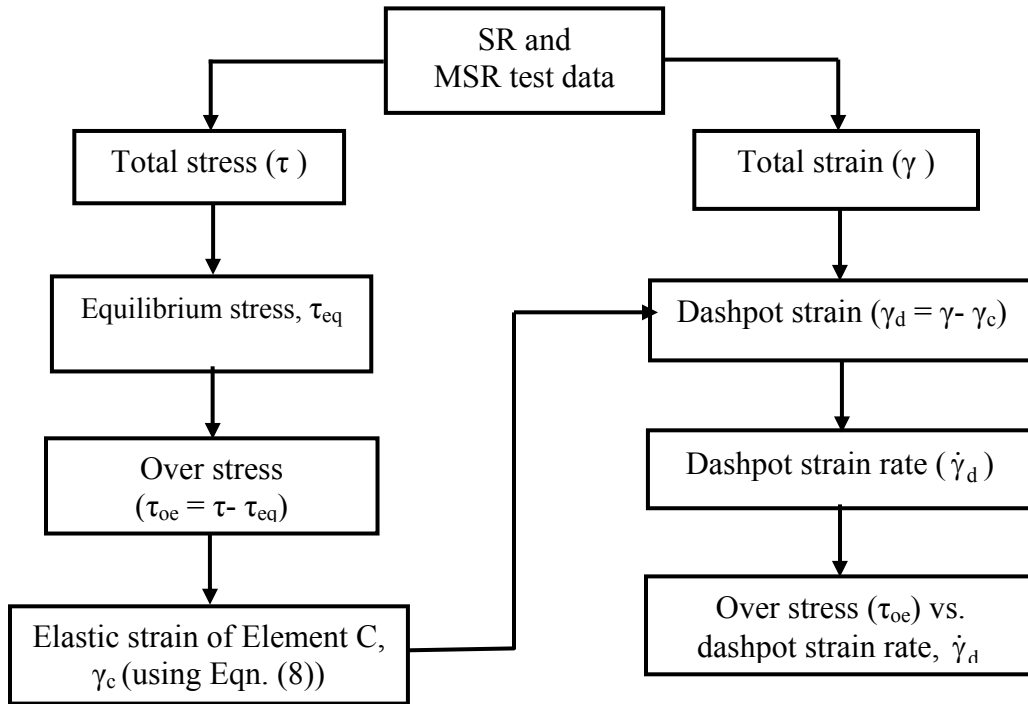
**[Figure 13]**



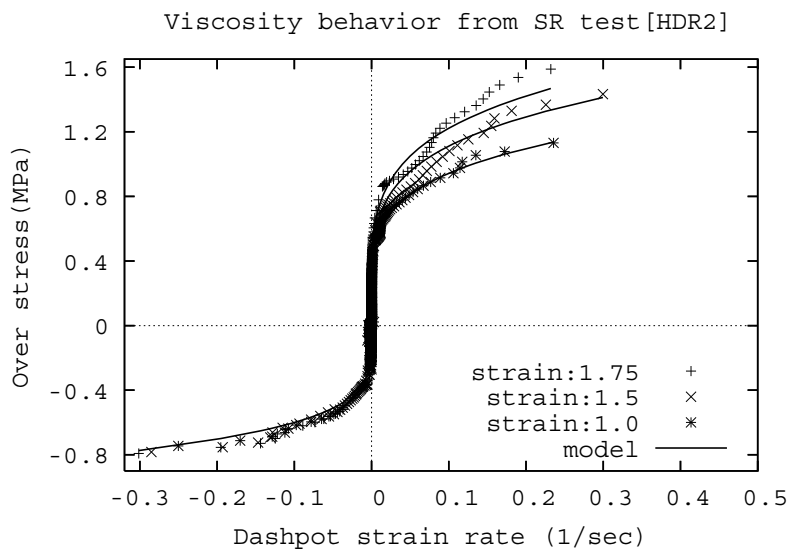
[Figure 14]



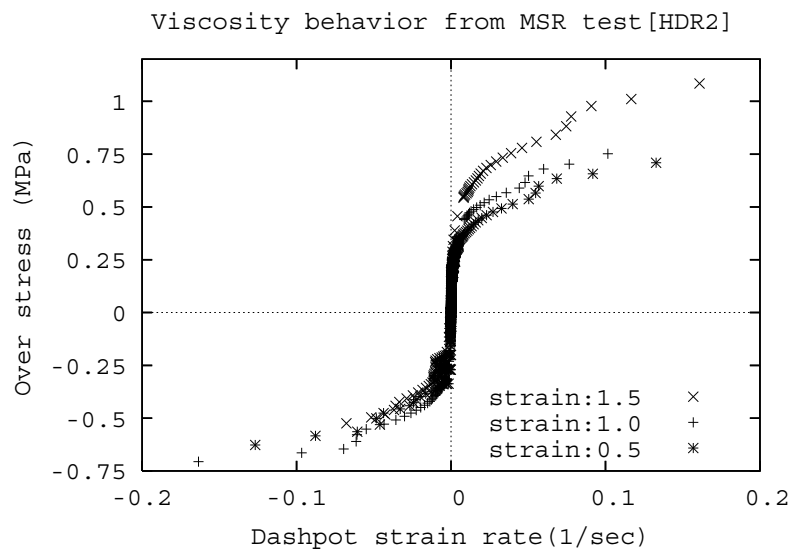
**[Figure 15]**



[Figure 16]

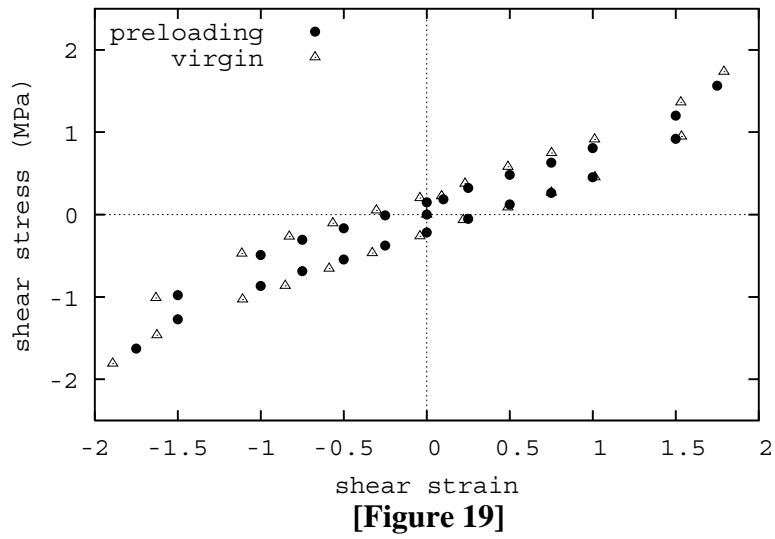


**[Figure 17]**



[Figure 18]

Equilibrium hysteresis [HDR2]



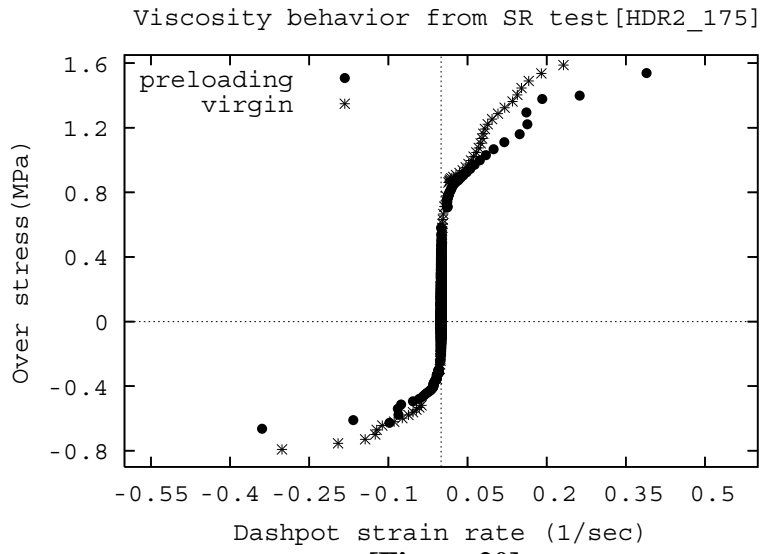


[Figure 20]

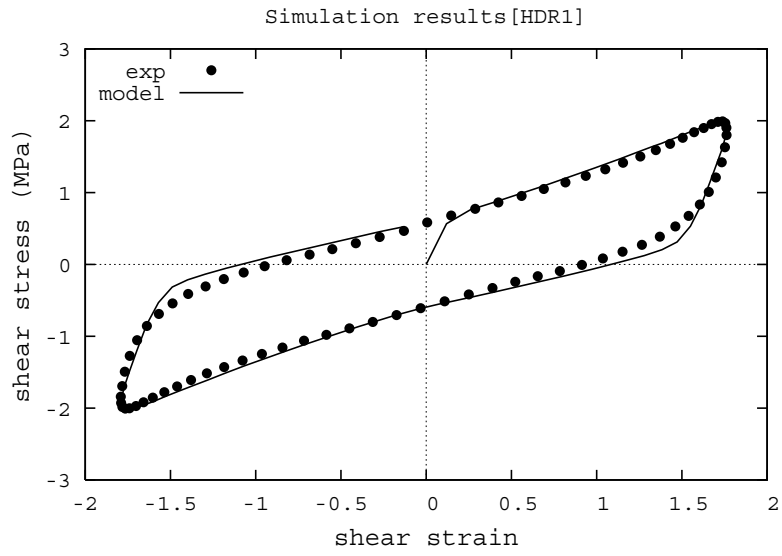


[Figure 21a]

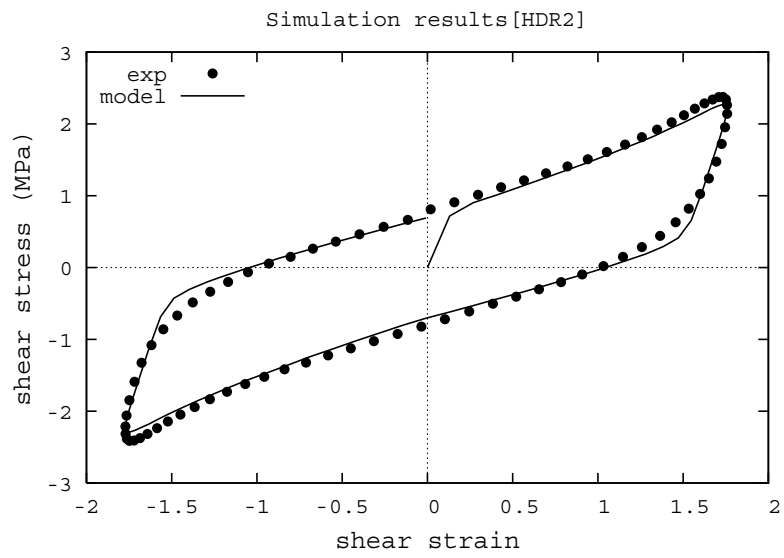


[Figure 21b]

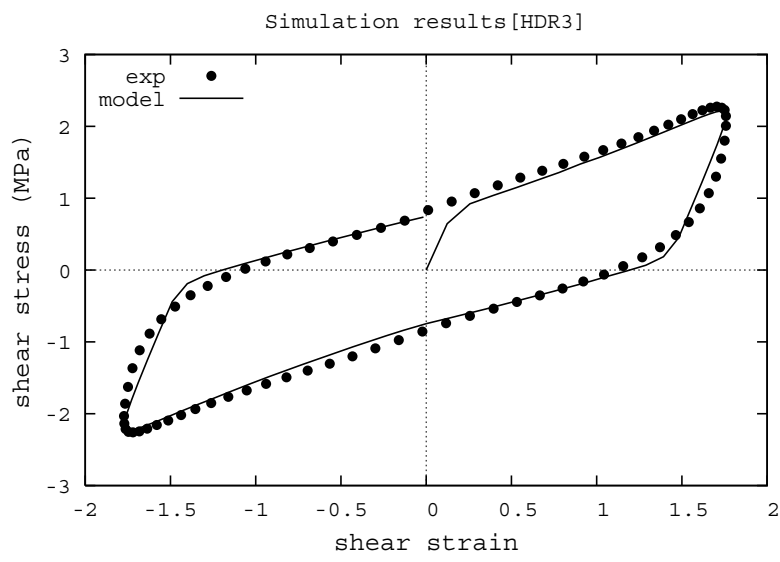


[Figure 21c]